

Chemistry A European Journal

 **Chemistry
Europe**
European Chemical
Societies Publishing

Accepted Article

Title: Non-emissive Ru(II) polypyridyl complexes as efficient and selective photosensitizers for the photooxidation of benzylamines

Authors: Gustavo Espino, Cristina Yagüe, Igor Echevarría, Mónica Vaquero, Jairo Fidalgo, Arancha Carbayo, Félix A. Jalón, Joao Lima, Artur Moro, and Blanca R. Manzano

This manuscript has been accepted after peer review and appears as an Accepted Article online prior to editing, proofing, and formal publication of the final Version of Record (VoR). This work is currently citable by using the Digital Object Identifier (DOI) given below. The VoR will be published online in Early View as soon as possible and may be different to this Accepted Article as a result of editing. Readers should obtain the VoR from the journal website shown below when it is published to ensure accuracy of information. The authors are responsible for the content of this Accepted Article.

To be cited as: *Chem. Eur. J.* 10.1002/chem.202001460

Link to VoR: <https://doi.org/10.1002/chem.202001460>

WILEY-VCH

FULL PAPER

Non-emissive Ru(II) polypyridyl complexes as efficient and selective photosensitizers for the photooxidation of benzylamines

Cristina Yagüe,^[a] Igor Echevarría,^[a] Mónica Vaquero,^{*,[a]} Jairo Fidalgo,^[a] Arancha Carbayo,^[a] Félix A. Jalón,^[b] Joao Lima,^[c] Artur Moro,^[c] Blanca R. Manzano^[b] and Gustavo Espino^{*,[a]}

[a] C. Yagüe, I. Echevarría, Dr. M. Vaquero, J. Fidalgo, Dr. A. Carbayo and Dr. G. Espino.
Departamento de Química, Facultad de Ciencias
Universidad de Burgos.
Plaza Misael Bañuelos s/n, 09001, Burgos, Spain.

E-mail: mvaquero@ubu.es, gespino@ubu.es

[b] Dr. F. A. Jalón and Dr. B. R. Manzano.
Departamento de Química Inorgánica, Orgánica y Bioquímica. Facultad de Químicas.
Universidad de Castilla-La Mancha, Avda. Camilo J. Cela 10, 13071 Ciudad Real, Spain.

[c] Dr. J.C. Lima and Dr. Artur Moro
LAQV-REQUIMTE, Departamento de Química, Faculdade de Ciências e Tecnologia,
Universidade NOVA de Lisboa, 2829-516 Caparica, Portugal.

Supporting information for this article is given via a link at the end of the document.

Abstract: Five new Ru(II) polypyridyl complexes bearing N-(arylsulfonyl)-8-amidoquinolate ligands and three of their biscyclometalated Ir(III) congeners have been prepared and employed as photocatalysts (PCs) in the photooxidation of benzylamines with O₂. In particular, the new Ru(II) complexes do not exhibit photoluminescence but they harvest visible light efficiently and are very stable in solution under irradiation with blue light. Their non-emissive behavior has been related to the low electrochemical energy gaps and rationalized on the basis of theoretical calculations (DFT analysis), which predict low S₀ ← T₁ energy values. Moreover, the Ru(II) complexes, despite being non-emissive, display excellent activities in the selective photocatalytic transformation of benzylamines into the corresponding imines. The presence of an electron withdrawing group (–CF₃) on the arene ring of the N-(arylsulfonyl)-8-amidoquinolate ligand improves the photocatalytic activity of the corresponding photocatalyst. Furthermore, all the experimental evidences, including Transient Absorption Spectroscopy measurements suggest that singlet oxygen is the actual oxidant. The Ir(III) analogues are considerably more photosensitive and consequently less efficient photosensitizers (PSs).

Introduction

Visible-light photocatalysis is a very attractive synthetic tool in as much as it uses visible light as the energy source for the construction of new C-C and C-heteroatom bonds in a green, efficient and selective manner. The mild conditions required in this type of methodology (room temperature and visible light) prevent side reactions from taking place and make it compatible with diverse functional groups present in the substrates. Besides, photocatalysis involves electronic excitation steps, which significantly change the reactivity of chemical compounds, allowing unique reaction pathways that afford non-conventional chemical products.^[1] In other words, photocatalysis relies on the ability of some heterogeneous semiconductors, organometallic complexes and organic dyes to harvest visible light and convert it

into chemical energy through the generation of unique reactive species.^[2] Although organic dyes do not produce heavy-metal waste, transition-metal photosensitizers (PSs) typically feature longer excited-state lifetimes, broader redox windows and require lower catalyst loadings.^[3] In particular, Ru(II) and Ir(III) polypyridyl complexes of the types [Ru(bpy)₃]²⁺ (bpy = 2,2'-bipyridine) and fac-[Ir(ppy)₃] (ppy = 2-phenylpyridine) are paradigmatic photosensitizers widely used in photocatalysis.^[4]

On the other hand, imines are important precursors or intermediates in the synthesis of nitrogen-containing compounds.^[5,6] Traditionally, they have been used as electrophiles towards different nucleophiles affording amines,^[7,8] α-amino nitriles^[9] and N-containing heterocycles.^[10]

Several methods are known for the preparation of imines: (a) condensation of amines and aldehydes; (b) oxidation of amines to imines using stoichiometric oxidants;^[11] (c) catalytic oxidation of primary and secondary amines;^[12,13] (d) photocatalytic oxidation of primary and secondary amines;^[14,15] and (e) photooxidative cross-coupling between amines and benzyl halides.^[16] Nevertheless, application of method (a) is sometimes limited by the formation of H₂O and the sensitivity of imines versus hydrolysis. Method (b) involves the use of corrosive oxidants and produces undesirable waste. Moreover, methods (a), (b) and (c) require high temperatures. On the other hand, the photocatalytic methods (d) and (e) are typically performed at room temperature and use O₂ as a clean and cheap oxidant source.^[17]

During the last years different homogeneous and heterogeneous photocatalytic systems have been described to obtain imines from benzylamines or dibenzylamines. It is worth mentioning the protocols based on Rh(I),^[18] Ir(III),^[19] Os(II)^[20] and Au(III)^[21] complexes, porphycene derivatives,^[22] porphyrin and Ru(II) porphyrin complexes,^[15] phenothiazine dyes^[17] and BODIPY derivatives^[23] as homogeneous photocatalysts. Remarkable heterogeneous photosensitizers are those based on carbon Quantum Dots,^[24] dye-sensitized TiO₂,^[25] Nb₂O₅,^[26] carbon nitride,^[27] WS₂ nanosheets,^[28] ZnIn₂S₄,^[29] carbazolic conjugated polymers^[30,31] and Ru-sensitized metal-organic frameworks.^[32] Nonetheless, some of these systems employ high temperatures

FULL PAPER

and O₂ pressures,^[24,27] some others use undesirable solvents (e.g.: benzene),^[18,26] or exhibit moderate selectivity.^[25,29,30] Polypyridyl Ru(II) complexes of the type [Ru(bpy)₃]²⁺ have been successfully employed as photocatalysts in multiple organic transformations.^[33] More specifically, they have also been used in aerial photooxidation reactions, in which they are efficient photosensitizers due to their ability to produce singlet oxygen (¹O₂), or radical anion superoxide (O₂^{•-}) from the ground state of molecular oxygen (³O₂). However, as far as we know the use of monocationic Ru(II) polypyridyl complexes of general formula [Ru(bpy)₂(N[^]N)]⁺ (N[^]N: monoanionic ligand) as photocatalysts has not been explored, even though they could exhibit high potential as light-harvesting antennas.^[34]

In this paper, we report on the design of new bis-heteroleptic Ru(II) and Ir(III) photosensitizers bearing N-(arylsulfonyl)-8-amidoquinolate ligands and on the successful evaluation of their photocatalytic properties in the smooth and selective oxidation of primary and secondary benzylamines using O₂ as the oxidant. Interestingly, we found that the new Ru(II) complexes display excellent photocatalytic activity, despite being non-emissive. An in-depth study of their photophysical and electrochemical properties supported by theoretical calculations is also provided.

Results and Discussion

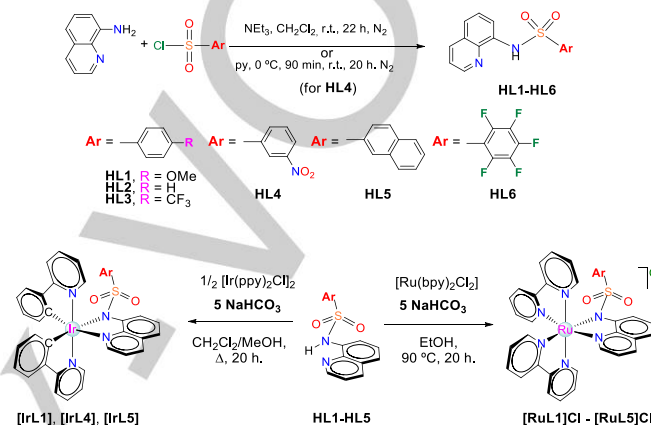
Synthesis and characterization of pro-ligands (HL1-HL6) and their Ru(II) and Ir(III) complexes

Pro-ligands HL1-HL6: The N-(quinolin-8-yl)arenesulfonamide pro-ligands **HL1-HL3**, **HL5** and **HL6** were prepared following a procedure adapted from those reported previously in the literature.^[35,36] This protocol consists in reacting 8-aminoquinoline with the appropriate sulfonyl chloride in the presence of triethylamine, in dichloromethane, at room temperature (Scheme 1). However, pro-ligand **HL4** was prepared by stirring 8-aminoquinoline in the presence of the corresponding sulfonyl chloride in pyridine at 0 °C and then at room temperature.^[37] Some of these pro-ligands have been previously used to prepare Ru(II) complexes of general formula [Ru(*p*-cym)Cl(N[^]N)] (N[^]N = **L1**, **L2** and **L3**)^[38] and [Ru(bpy)(SCN)(N[^]N)] (N[^]N = **L1**, **L2**).^[39]

Synthesis of the ruthenium complexes. The new Ru(II) complexes [RuL1]Cl-[RuL5]Cl of general formula *rac*-[Ru(bpy)₂(N[^]N)]Cl (N[^]N = **L1-L5**, i.e.: deprotonated **HL1-HL5**) were prepared by refluxing an ethanol solution of the starting material *rac-cis*-[Ru(bpy)₂Cl₂].2H₂O and the pro-ligands **HL1-HL5** in the presence of NaHCO₃ (Scheme 1). We failed to obtain the expected complex with **L6** as a pure product. Instead, we obtained a mixture of the desired product and the side-product derived from ethanolysis of the F atom in the *para* position (replacement of the F atom with a -OEt group, Table S11 and Scheme S11).^[40] All the Ru(II) derivatives exhibit C₁-symmetry and were isolated as racemic mixtures in the form of dark red solids which are air- and moisture-stable.

Synthesis of the iridium complexes. The neutral Ir(III) complexes of general formula *rac*-[Ir(ppy)₂(N[^]N)] (N[^]N = **L1**, **L4** and **L5** for [IrL1], [IrL4] and [IrL5], respectively) were synthesized by refluxing a mixture of *rac*-[Ir(μ-Cl)(ppy)₂]₂ and the appropriate

pro-ligand in the presence of an excess of NaHCO₃ in CH₂Cl₂/MeOH (Scheme 1). These photosensitizers were used in the photocatalytic tests for comparison purposes. Complex [IrL1] and other related derivatives had been previously reported by Aoki.^[41] Moreover, the reaction of *rac*-[Ir(μ-Cl)(ppy)₂]₂ with ligand **HL6** gave a mixture of the expected product along with the respective methanolysis derivative in which the F atom in *para* has been substituted by a -OMe group (see Table S12 and Scheme S12).^[34,42,43] The Ir(III) derivatives also exhibit C₁-symmetry and were isolated as racemic mixtures in the form of air- and moisture-stable yellow solids.



Scheme 1. Synthesis of the pro-ligands **HL1-HL6**, the new Ru(II) polypyridyl complexes [RuL1]Cl-[RuL5]Cl and the Ir(III) derivatives [IrL1], [IrL4] and [IrL5]. All the complexes are obtained as racemic mixtures, although only the Δ enantiomers are shown.

Characterization of the new complexes

The composition and structure of these compounds were determined by multinuclear and 2D NMR spectroscopy, together with high resolution mass spectrometry (HR-ESI), IR spectroscopy and elemental analysis (See SI). The ¹H NMR spectra of the Ru(II) complexes were recorded in CDCl₃ at 25 °C and exhibit the following distinctive general features: (a) The N-H peaks observed as broad singlets above 9.2 ppm for pro-ligands **HL1-HL5** are missing in the spectra of complexes [RuL1]Cl-[RuL5]Cl; (b) The resonances for both the bipyridyl and the N-(arylsulfonyl)-8-amidoquinolate ligands are displaced with regard to those of *rac-cis*-[Ru(bpy)₂Cl₂] and the free pro-ligands, respectively; (c) Four sets of peaks are identified for the four inequivalent pyridyl rings in agreement with the asymmetric nature of these derivatives. The HR-ESI(+) spectra of complexes [RuL1]Cl-[RuL5]Cl displayed envelope peaks compatible with the expected monocationic species of formulae [Ru(bpy)₂(N[^]N)]⁺ (see the spectrum for [RuL4]Cl in Figure S11). The characterization data of the Ir(III) complexes are gathered in the supporting information (see the HR-ESI(+) mass spectrum for [IrL5] in Figure S12).

Crystal Structure. Attempts to get single crystals of the chloride salts of the Ru complexes were fruitless. Conversely, we obtained single crystals of [RuL4]PF₆ suitable for X-Ray diffraction by slow diffusion of an aqueous solution of NH₄PF₆ into a solution of

FULL PAPER

[RuL4]Cl in methanol. The ORTEP diagram for cation complex of (Λ)-**[RuL4]PF₆** is shown in

Figure 1, whereas selected bond distances and angles and crystallographic refinement parameters are collected in Tables SI3 and SI4. The unit cell consists of two pairs of enantiomeric cation complexes (Λ and Δ) plus four PF₆[−] counteranions.

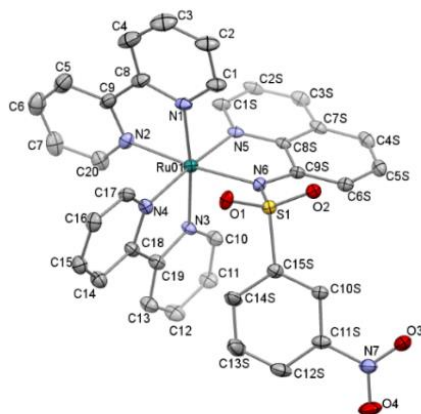


Figure 1. ORTEP diagram for (Λ)-**[RuL4]PF₆**. The PF₆[−] counteranion and hydrogen atoms have been removed for the sake of clarity. Thermal ellipsoids are shown at the 30% probability level.

The coordination polyhedron exhibits a slightly distorted octahedral geometry and it is formed by the three expected (Λ)-chelate ligands: two bpy and the formally anionic **L4**. The Ru-N_{py} bond distances are standard (2.045–2.058 Å) and shorter than the Ru-N bond lengths determined for **L4**. More specifically, the latter (Ru1-N5, 2.062 and Ru1-N6, 2.124 Å) are similar to those reported for a related complex with a monoanionic ligand of the type N-(carboxyaryl)amidoquinolate.^[34] Moreover, the N-Ru-N chelate angles compare well with those reported for similar derivatives (78.30°–80.00°).^[34] The 3D crystal network displays dimeric entities formed by pairs of enantiomers (Λ , Δ), which interact one to another through several hydrogen bonds: C1H1---O3; C10SH10S---O2, C6SH6S---O2 (Figure SI3).

Photostability of the photosensitizers

Photostability is a highly desirable property in the context of photocatalytic reactions. In fact, the overall photocatalytic performance of metallo-organic complexes is primarily limited by their photolysis, which is thought to occur through the photoinduced solvolysis of the metal-(Λ)-bonds.^[44] Hence, the stability of complexes **[RuL1]Cl**–**[RuL5]Cl** and **[Ru(bpy)₃]Cl₂** (henceforth denoted as **[1]Cl₂** or **[1]²⁺**) in CD₃CN (1.4·10^{−2} M), first in the dark, and then under irradiation with blue light (LED, λ_{irr} = 460 nm, 24 W) was monitored by ¹H NMR over a period of 24 h in a NMR tube capped with a septum under atmospheric air (see Figures SI4–SI9). All the compounds are utterly stable in the dark. On the other hand, complexes **[RuL1]Cl**–**[RuL3]Cl** and **[1]Cl₂** exhibited moderate photostability in deuterated acetonitrile, with decomposition values of 17 %, 28 %, 16 % and 19 % after 24 h, respectively (see Figures SI4–SI6 and SI9). Moreover, **[RuL4]Cl** showed no symptoms of photodegradation and **[RuL5]Cl** displayed only 2 % of decomposition after 24 h under irradiation (see Figures SI7 and SI8, respectively). Thus, it seems that the

aryl substituent on the sulphonamide group influences considerably the photostability of these derivatives. The Ir(III) complexes are markedly less stable under light exposure. Indeed, complexes **[IrL1]** and **[IrL5]** decompose completely after 24 and 6 h respectively, while complex **[IrL4]** exhibit a 26 % photodegradation after 24 h (see Figures SI10–SI12).

Electronic absorption properties

The UV-Vis absorption spectra of the above-mentioned Ru and Ir complexes (see Figure 2 and data in Table 1) were recorded in acetonitrile solutions (5·10^{−5} M) at 25 °C. In particular, the absorption spectra of complexes **[RuL1]Cl**–**[RuL5]Cl** are virtually identical and show two intense absorption bands centred at about 247 and 293 nm, which can be attributed to singlet spin-allowed ligand centred (¹LC) transitions involving both bipyridyl ligands and the ancillary **L1**–**L5** ligands. Two weak, unstructured and broad bands are also observed in the intervals 320–380 nm and 381–600 nm, approximately (see Figure 2 and Table 1). These bands are assigned to spin-allowed ¹MLCT, ¹LLCT and spin-forbidden ³MLCT (singlet to triplet d π (Ru) \rightarrow π^* (N \wedge N)), ³LLCT (singlet to triplet, ³ π (N \wedge N) \rightarrow π^* (C \wedge N)) and ³LC (singlet to triplet ³ $\pi \rightarrow \pi^*$) transitions.

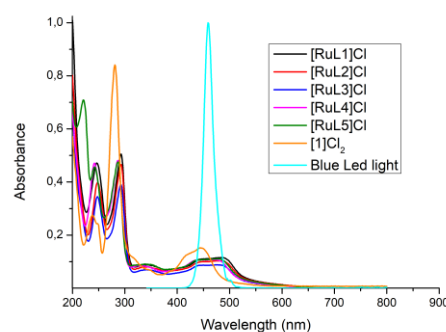


Figure 2. UV-Vis absorption spectra of **[RuL1]Cl**–**[RuL5]Cl** and **[1]Cl₂** (5·10^{−5} M) in acetonitrile at 25 °C and emission spectrum of the blue LED light used in photocatalysis.

Table 1. Wavelengths (λ_{abs}) and molar extinction coefficients (ϵ) at the absorption maxima and relative maxima in the UV-Vis spectra of complexes **[RuL1]Cl**–**[RuL5]Cl** and **[1]Cl₂** measured in acetonitrile at 25 °C.

Complex	λ_{abs} [nm]	ϵ [M ^{−1} cm ^{−1}]
[RuL1]Cl	247, 292, 340, ^[a] 483 ^[a]	0.471, 0.505, 0.088, ^[a] 0.115 ^[a]
[RuL2]Cl	248, 293, 344, ^[a] 479 ^[a]	0.398, 0.466, 0.080, ^[a] 0.103 ^[a]
[RuL3]Cl	248, 292, 342, ^[a] 482 ^[a]	0.345, 0.389, 0.070, ^[a] 0.088 ^[a]
[RuL4]Cl	242, 287, 333, ^[a] 460 ^[a]	0.471, 0.481, 0.085, ^[a] 0.107 ^[a]
[RuL5]Cl	221, 242, 287, 334, ^[a] 456 ^[a]	0.709, 0.456, 0.476, 0.09, ^[a] 0.108 ^[a]
[1]Cl₂	238, 282, 445	0.275, 0.838, 0.152

^[a] Midpoint of broad absorption band.

In comparison with the reference compound **[1]²⁺**, the replacement of one bpy ligand on the former with the anionic ligands **L1**–**L5** broadens and shifts to the red the absorption profile

FULL PAPER

of complexes **[RuL1]Cl**–**[RuL5]Cl** and consequently improves visible light harvesting.^[34] The emission spectrum of the blue light used in the photooxidation assays is also included in Figure 2 to show the excellent overlapping with the absorption spectra of our **PSs**. In other words, we conclude that excitation of our **PSs** is optimal under this light source ($\lambda = 460$ nm).

Photoluminescence spectroscopy

Attempts to record the emission spectra for the new Ru(II) complexes in deoxygenated acetonitrile or DMSO solutions (10^{-5} M) at different excitation wavelengths and room temperature failed. Therefore, these compounds are practically non-emissive at room temperature in contrast to the reference complex **[1](PF₆)₂**, which features moderate PLQY (Photoluminescence Quantum Yield)^[45] and long excited-state lifetime.^[3] For this reason, photoluminescence quantum yields and excited state lifetimes could not be determined for the Ru-**PCs**. The iridium derivatives **[IrL1]**, **[IrL4]** and **[IrL5]** exhibit weak emission properties but PLQY and excited state lifetimes could neither be experimentally determined precisely due to the poor photostability of these derivatives. Non-emissive complexes at room temperature have scarcely been used as photosensitizers, likely due to the widely accepted premise that a high PLQY and a long-excited state lifetime ensure good performance to a particular photocatalyst (**PC**). By contrast, we postulate that our non-emissive Ru and Ir complexes could exhibit photocatalytic activity, assuming efficient intersystem crossing typical of d⁶-Ru(II) polypyridyl and d⁶-Ir(III) biscyclometalated complexes, and provided that the photosensitizing process is kinetically faster than the non-radiative decay. More precisely, in the context of O₂-mediated photooxidation reactions, the preliminary condition for a **PC** should be that the short-lived excited state of the **PC** (**PC**^{*}) undergoes deactivation through interaction with O₂ faster than non-radiative decay.

Electrochemical behaviour

The redox potentials of **[RuL1]Cl**–**[RuL5]Cl** and **[1]Cl₂** were determined in degassed acetonitrile solutions by cyclic voltammetry (CV) using [nBu₄N][PF₆] as supporting electrolyte and glassy carbon as the working electrode (see cyclic voltammograms in Figure SI13 and SI14, respectively).^[46] Potentials are given with respect to the ferrocene/ferrocenium (Fc⁺/Fc) couple. Figure 3 illustrates the cyclic voltammogram of **[RuL3]Cl** as a representative example of all the new Ru dyes and that of **[1]Cl₂** for comparison purposes. Thus, in the anodic region all the photosensitizers exhibit an irreversible oxidation peak between +0.54 and +0.75 V, which is attributed to the oxidation of the chloride counteranion (Cl[−] → Cl₂). In addition, all the **PSs** display a reversible redox peak between +0.22 and +0.30 V versus Fc⁺/Fc, which is assigned to the Ru^{II}–(N[^]N) (N[^]N = **L1**–**L5**) environment (see the hybrid topology of the HOMO level in DFT calculations below,

Figure 4 and Figure SI15). This involves a strong cathodic shift relative to the reference compound **[1]²⁺** which, on the other hand, exhibits a localized metal-centred Ru^{III}/Ru^{II} redox couple. This shift is reasonable taking into account the anionic nature and strong electron donating character of ligands **L1** to **L5**.^{[34],[47]} Contrary to **[1]Cl₂**, all the new dyes exhibit an extra irreversible oxidation peak in the range between +1.26 and +1.36 V versus

Fc⁺/Fc, which is ascribed again to the Ru^{II}–(N[^]N) region (N[^]N = **L1**–**L5**), and produces species of the type [Ru^{III}–(N[^]N)]³⁺ (*vide infra* and see Scheme 2). In the cathodic region, all the new complexes feature two common reversible peaks: the first one between −1.83 and −1.92 V is imputed to the reduction of one bipyridyl ligand ([Ru^{II}(bpy)₂(N[^]N)]⁺ → [Ru^{II}(bpy[−])(bpy)(N[^]N)]⁰) and the second one, between −2.07 and −2.24 V, is attributed to the reduction of the other bipyridyl ligand ([Ru^{II}(bpy[−])(bpy)(N[^]N)]⁰ → [Ru^{II}(bpy[−])(bpy[−])(N[^]N)][−])^[48] in agreement with the topology of the LUMO level that is based on bpy(π*) orbitals (See theoretical calculations below). In the voltammogram of **[RuL4]Cl**, there are extra peaks assigned to the typical reduction of the −NO₂ group.^[49] The electrochemical band gaps ($\Delta E_{1/2}$) calculated from the first reversible oxidation potential and the first reversible reduction potential for the new **PCs** (2.07–2.22 V) are lower than for **[1]²⁺** (2.61 V) and anticipate a lower S₀ ← T₁ energy for the new Ru complexes relative to **[1]²⁺** (Table 2). Cyclic voltammograms for **[IrL1]**, **[IrL4]** and **[IrL5]** are also given in Figure SI4 and Table SI5.

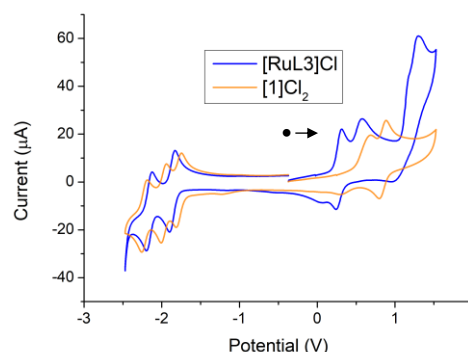


Figure 3. Cyclic voltammograms of complexes **[RuL3]Cl** and **[1]Cl₂** in acetonitrile solution (10^{-3} M), using 0.1 M [nBu₄N][PF₆] as supporting electrolyte and recorded with scan rate of 0.10 V·s^{−1}. The starting and final potentials (E_i, E_f) are indicated by (•) and the sense of the scan (clockwise) is indicated by the arrow.

Table 2. Cyclic voltammetry data referenced to Fc⁺/Fc in acetonitrile solution (10^{-3} M).^[a]

Complex	E ^{ox} _{1/2} (V)	E ^{red} _{1/2} (V)	ΔE _{1/2} (V)
[1]Cl₂	+0.89 (r)	−2.17 (r)	2.61
	+0.67 (ir) ^[b]	−1.82 (r)	
		−1.72 (r)	
[RuL1]Cl	+1.28 (ir)	−2.07 (r)	2.07
	+0.56 (ir) ^[b]	−1.83 (r)	
	+0.24 (r)		
[RuL2]Cl	+1.26 (ir)	−2.19 (r)	2.09
	+0.65 (ir) ^[b]	−1.87 (r)	
	+0.22 (r)		
[RuL3]Cl	+1.30 (ir)	−2.16 (r)	2.15
	+0.58 (ir) ^[b]	−1.87 (r)	
	+0.28 (r)		
[RuL4]Cl	+1.36 (ir)	−2.24 (r)	2.22
	+0.75 (ir) ^[b]	−1.92 (r)	
	+0.30 (r)	−1.38 (ir) ^[c]	
		−1.20 (ir) ^[c]	
[RuL5]Cl	+1.28 (ir)	−2.17 (r)	2.09
	+0.59 (ir) ^[b]	−1.86 (r)	
	+0.23 (r)		

^[a] Measured using 0.1 M [nBu₄N][PF₆] as supporting electrolyte and a scan rate of 0.10 V·s^{−1} (r = reversible, ir = irreversible). ^[b] Oxidation of Cl[−]. ^[c] Reduction of the −NO₂ group. ΔE_{1/2} = E^{ox}_{1/2} − E^{red}_{1/2} = first reversible oxidation potential − first reversible reduction potential.

FULL PAPER

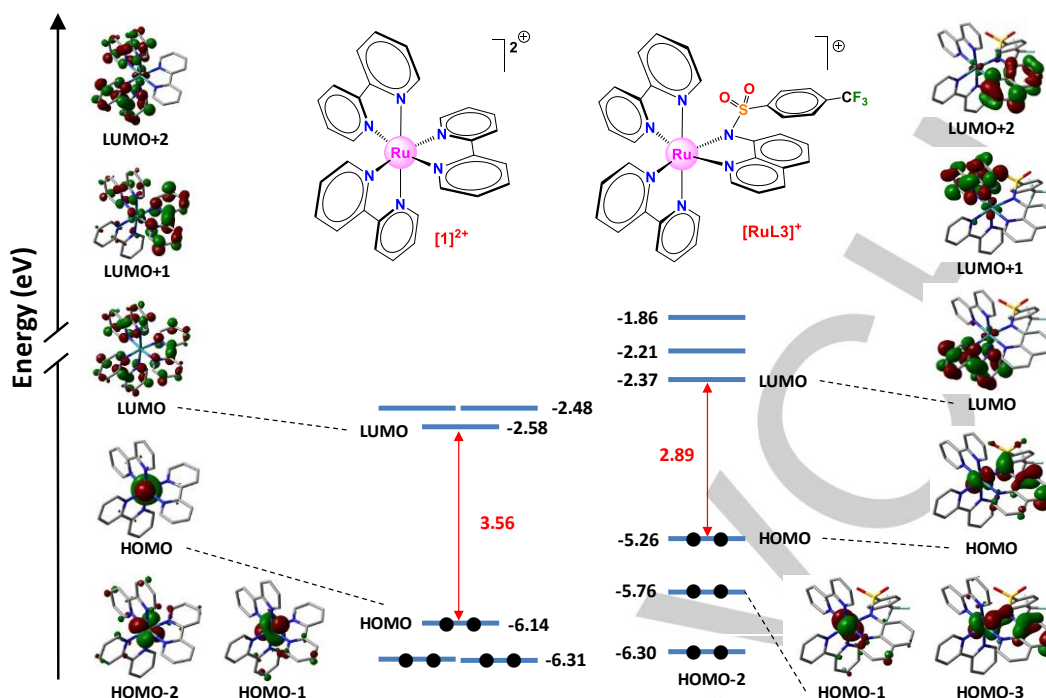
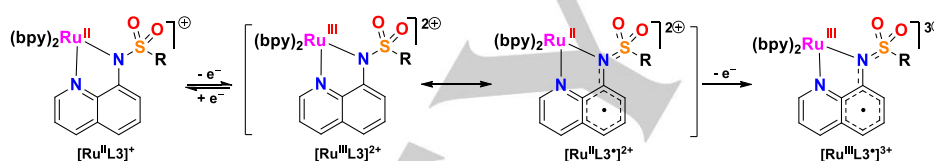


Figure 4. Schematic representation showing the energies and the isovalue contour plots calculated for the frontier molecular orbitals of $[1]^{2+}$ and $[RuL3]^+$. HOMO-3 is shown instead of HOMO-2 for $[RuL3]^+$.



Scheme 2. Illustration of the oxidation processes for the new Ru(II) complexes. $[Ru^{III}L3]^{2+}$ and $[Ru^{II}L3]^+$ are the canonical forms proposed for the first oxidation event, while $[Ru^{III}L3]^{3+}$ is the species formed upon the second electron oxidation event.

Theoretical calculations

Density functional theory (DFT) and time-dependent DFT (TD-DFT) calculations were performed on the cations of complexes $[RuL1]^+-[RuL3]^+$ and also for the reference complex $[1]^{2+}$ to get a better understanding of the electrochemical and photophysical properties discussed above. Calculations were carried out at the B3LYP/(6-31GDP+LANL2DZ) level including solvent effects (CH₃CN) (see the Experimental Section for details). Calculations predict a near-octahedral structure for cations $[RuL1]^+-[RuL3]^+$ and $[1]^{2+}$ in their ground electronic state (S_0), in good agreement with the crystal structure of $[RuL4]PF_6$.

Figure 4 features the isovalue contour plots calculated for the molecular orbitals (MOs) of $[1]^{2+}$ and $[RuL3]^+$ (as an example) at their electronic ground state (S_0). The HOMO and degenerate HOMO-1 and HOMO-2 of $[1]^{2+}$ are filled, mainly located in the metal centre and exhibit a non-bonding character, whereas the empty LUMO and degenerate LUMO+1 and LUMO+2 are located in the bpy ligands and display a non-bonding character as well. Hence, the Ru-N interactions in $[1]^{2+}$ exhibit mainly a σ -bonding character with negligible π -bonding nature. By contrast, the HOMO and HOMO-3 of $[RuL3]^+$ consist of a mixture of d_{π} orbitals of Ru(II) and π orbitals of the amidoquinolate fragment of **L3** with π -antibonding (HOMO) and π -bonding (HOMO-3) character at the Ru-N_{amido} interface, respectively (see Figure S115). These

topologies imply a good covalent Ru($d\pi$)-L3(π) molecular orbital overlap, as suggested by Rochford *et al.*, for isostructural Ru(II) complexes with N-carboxyamidoquinolate ligands.^[34] Moreover, the HOMO of $[RuL3]^+$ is greatly destabilized (0.88 eV) compared to the corresponding orbital of $[1]^{2+}$, which can be imputed to the higher electron donor ability of the formally anionic **L3** ligand versus bpy in $[1]^{2+}$. This matches well with the experimental $E^{ox}_{1/2}$ values (Table 2), since the oxidation of $[RuL3]^+$ is easier than that of $[1]^{2+}$. Furthermore, the first oxidized form of $[RuL3]^+$ is better described by the combination of two canonical structures: the first one involving a Ru^{III} centre, $[Ru^{III}L3]^{2+}$ and the second one a radical **L3**[•] ligand, $[Ru^{II}L3^{\bullet}]^{2+}$ (see Scheme 2).^[34] Rationally, the second oxidation event experimentally observed for $[RuL3]^+$, and its analogues, likely leads to the formation of species of the type $[Ru^{III}L3^{\bullet}]^{3+}$ (see Scheme 2). In addition, the contribution of the aryl groups (-Ar) to the frontier molecular orbitals (MO) and, in particular to HOMO-3, responsible for the π (Ru-L) bonding overlapping, is negligible, revealing an ineffective conjugation between the aryl groups and the fluorogenic backbone. This, in turn, is consistent with the weak effect experimentally observed on the photophysical and electrochemical properties of the new ruthenium compounds exerted by the different aryl groups.

The LUMO of $[RuL3]^+$ is fully located over a bpy ligand and is also destabilized relative to the LUMO of $[1]^{2+}$, but to a lesser extent (0.21 eV), in agreement with the experimental $E^{red}_{1/2}$ values (Table 2). Consequently, the HOMO-LUMO band gap is narrower for

FULL PAPER

[RuL3]⁺ than for **[1]²⁺** (2.89 vs 3.56 eV) in harmony with the electrochemical band gaps (see $\Delta E_{1/2}$ in Table 2). Moreover, the low lying excited states of complexes **[RuL1]⁺**-**[RuL3]⁺** and **[1]²⁺** were calculated at the optimized geometries of the ground state (S_0) by mean of the time-dependent DFT (TD-DFT) approach. Table S16 summarizes the vertical excitation energies calculated for the first three singlets and triplets, together with their molecular orbital description and electronic nature. A summary of these results is graphically shown in Figure 5. The three first triplet states of **[1]²⁺** are originated from HOMO \rightarrow LUMO+1, HOMO \rightarrow LUMO+2 and HOMO \rightarrow LUMO excitations, respectively, and all of them display ³MLCT character. On the contrary, the three first triplet states of **[RuL1]⁺**-**[RuL3]⁺** essentially stem from HOMO \rightarrow LUMO, HOMO \rightarrow LUMO+2 and HOMO \rightarrow LUMO+1 excitations, respectively, and are very close in energy. In particular, the HOMO \rightarrow LUMO excitation for the new dyes involves the promotion of one electron from the Ru-(N⁺N) ((N⁺N) = **L1**, **L2**, **L3**) (HOMO) environment to a bpy ligand (LUMO), and hence the T_1 excited state exhibits a mixed ³MLCT/³LLCT character. Besides, the first three triplet states for **[RuL1]⁺**-**[RuL3]⁺** display lower E_0 values ($S_0 \leftarrow T_1$) than those of **[1]²⁺** in agreement with the strong destabilization of the HOMO when a bpy ligand is replaced with a formally anionic N-(arylsulfonyl)-8-amidoquinolate ligand (Figure 5). These calculations support the energy-gap law [$k_{nr} \propto \exp(-E_0)$] as the main hypothesis for the non-emissive behaviour of the new dyes.^[34,50] According to this empirical law, the rate constant for non-radiative decay (k_{nr}) increases exponentially with a decreasing $S_0 \leftarrow T_1$ energy (E_0).

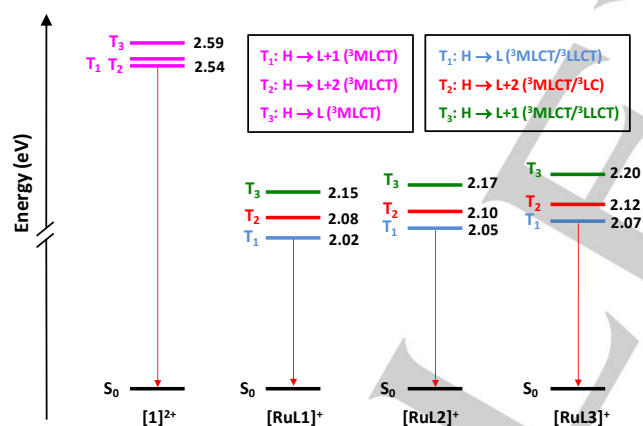


Figure 5. Energy diagram showing the energy values calculated for the lowest-energy triplet excited states (T_n) of complexes **[RuL1]⁺**-**[RuL3]⁺** and **[1]²⁺**. Different colours are used to display the different electronic nature of the T_n states according to the chromatic key in the boxes.

Photocatalytic Oxidation of Benzylamines

Next, we decided to evaluate the photosensitizing properties of the new Ru(II) and Ir(III) complexes in the photooxidation of benzylamines, using CH₃CN as solvent as previously reported in the literature.^[23,51] First of all, we chose benzylamine (**1a**) as model substrate and **[RuL1]Cl** as the photosensitizer (0.1 % mol, S/C = 1000) and irradiated a solution of both in acetonitrile with blue light ($\lambda = 460$ nm) under an O₂ atmosphere (1 atm) at room temperature during 14 hours. To our delight, we observed full

conversion of **1a** into the imine **2a** (entry 1, Table 3). In addition, the transformation took place with excellent selectivity towards the oxidative coupling product (**2a**), since neither overoxidation products (e.g.: benzonitrile, benzamide, N-benzylhydroxylamine, benzaldehyde oxime,^[52] N-benzylidene-benzylamine N-oxide (nitron), or N-benzylbenzamide), nor hydrolysis products (benzaldehyde) were detected (see Scheme S13).

Table 3. Photocatalytic oxidative coupling of benzylamine **1a** with **[RuL1]Cl** and control experiments.^[a]

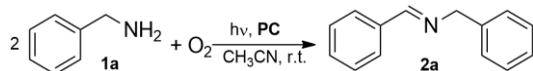
Entry	Conditions	Yield (%)
1	[RuL1]Cl , O ₂ , light	> 99
2	[RuL1]Cl , O ₂ , no light	7
3	No PC , O ₂ , light	5
4	[RuL1]Cl , N ₂ , light	12
5	[RuL1]Cl , O ₂ , light, TEMPO ^b	96
6	[RuL1]Cl , O ₂ , light, DABCO ^c	5

[a] Reaction conditions: Benzylamine **1a** (10 mM), **[RuL1]Cl** (10⁻² mM, 0.1 mol %), CH₃CN (0.5 mL) at room temperature, under a saturated atmosphere of either O₂ or N₂ (1 atm) and under irradiation with blue light (LED, $\lambda = 460$ nm, 24 W) during 14 h in a septum-capped tube. Conversion yields were determined by ¹H NMR analysis of the crude mixture as average values of at least two independent experiments. Overoxidation and/or hydrolysis products were not detected in any case. [b] TEMPO (11 mM). [c] DABCO (11 mM).

Control experiments verified the participation of O₂ and the photocatalytic nature of this oxidation process, since oxygen, light irradiation and the photosensitizer are all essential to accomplish the transformation of **1a** into **2a** (entries 2, 3 and 4, Table 3). In addition, an experiment in the presence of 2,2,6,6-tetramethyl-1-piperidinyloxy (TEMPO, entry 5, Table 3), a O₂⁻ scavenger,^[53] gave a yield of 96%. On the contrary, an experiment in the presence of 1,4-diazabicyclo[2.2.2]octane (DABCO, entry 6, Table 3), a singlet oxygen quencher,^[8] suppressed almost quantitatively the oxidative coupling. These results suggest that ¹O₂ is the actual oxidant agent and rule out the participation of superoxide in the mechanism of the reaction.

Then, the new Ru(II) complexes and their Ir(III) counterparts were tested as photocatalysts in the oxidative coupling of benzylamine (**1a**) using the above-mentioned conditions. Complex **[1]Cl₂** was also included in this screening with comparative purposes. Close to quantitative transformations to the imine **2a** were observed after 14 hours for **[RuL1]Cl**-**[RuL3]Cl**, **[RuL5]Cl** and **[1]Cl₂** (see entries 1-3, 5 and 9, Table 4). On the other hand, for **[IrL1]** and **[IrL5]** moderate yields of 70 % and 59 % were determined (entries 6 and 8, Table 4). The worse performance of these Ir(III) **PCs** compared to the Ru(II) analogues could be related to the lower photostability of the formers in comparison to the Ru **PCs**.

FULL PAPER

Table 4. Catalyst screening in the photocatalytic oxidative self-coupling of benzylamine **1a**.^[a]

Entry	Photocatalyst	Time (h)	Yield (%)
1	[RuL1]Cl	14	99
2	[RuL2]Cl	14	94
3	[RuL3]Cl	14	> 99
4	[RuL4]Cl	14	5
5	[RuL5]Cl	14	> 99
6	[IrL1]	14	70
7	[IrL4]	14	3
8	[IrL5]	14	59
9	[1]Cl ₂	14	> 99
10	[RuL1]Cl	6	78
11	[RuL2]Cl	6	75
12	[RuL3]Cl	6	91
13	[RuL5]Cl	6	66
14	[RuL3]Cl	1	69 ^[b]
15	[RuL3]Cl	2	97 ^[b]
16	[RuL3]Cl	1	96 ^{[b],[c]}

[a] Reaction conditions: benzylamine **1a** (10 mM), **PC** (10⁻² mM, 0.1 mol %), CH₃CN (0.5 mL) at room temperature, under a saturated atmosphere (1 atm) of O₂ and under irradiation with blue light (LED, λ = 460 nm, 24 W) during the indicated time in a septum-capped tube. Conversion yields were determined by ¹H NMR analysis of the crude mixture as average values of at least two independent experiments. Overoxidation and/or hydrolysis products were not detected in any case. [b] [RuL3]Cl (1 mol %). [c] Reaction performed in CD₃CN.

Moreover, the two complexes with a nitro group in the sulphonamide ligand, [RuL4]Cl and [IrL4], provided very low yields (entries 4 and 7 in Table 4), suggesting that the presence of this functional group deactivates the excited state of the respective **PC** as previously reported.^[54–57] Further experiments were carried out for the active Ru(II) **PCs** decreasing the reaction time until 6 h to identify the most efficient **PC** and to establish possible structure-activity relationships (entries 10–13 in Table 4). Thus, similar results were obtained for [RuL1]Cl, [RuL2]Cl and [RuL5]Cl, whereas for [RuL3]Cl the yield was remarkably higher which suggests that the presence of the electron-withdrawing group –CF₃ is beneficial for the reaction rate in some way. Then, the catalyst loading of [RuL3]Cl was increased up to 1 mol % to show that high yields of **2a** can also be obtained at low reaction times (entries 14 and 15 in Table 4). Besides, we demonstrated that the yield of **2a** is higher when the reaction is performed in CD₃CN relative to CH₃CN (compared entries 14 and 16 in Table 4), which is consistent with the participation of ¹O₂ as the actual oxidant since the lifetime of this species is longer in deuterated

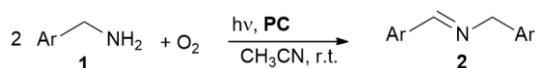
solvents.^{[58],[59]} Conclusively, complexes [RuL3]Cl and [RuL5]Cl were selected for additional experiments due to their good performance ([RuL3]Cl) and a combination of good photostability and good activity ([RuL5]Cl).

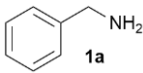
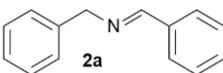
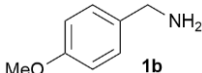
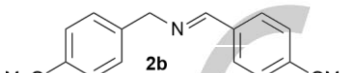
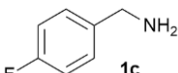
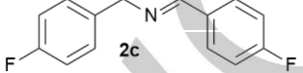
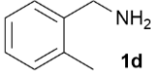
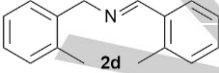
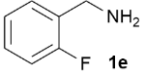
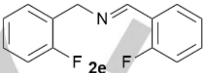
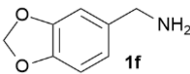
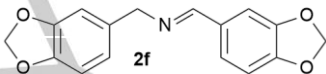
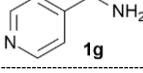
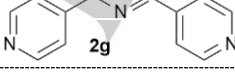
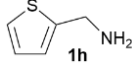
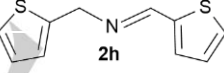
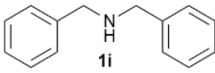
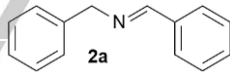
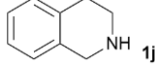
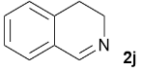
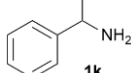
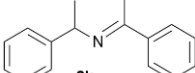
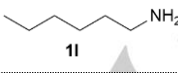
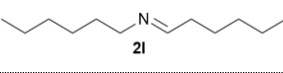
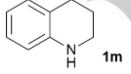
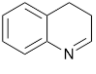
To demonstrate the validity of this photocatalytic protocol, the optimized conditions were applied to different primary and secondary benzylamines (**1b–1m**) in the presence of either [RuL3]Cl or [RuL5]Cl (Table 5). Thus, primary benzylamines **1b–1f** with both electron-donor or electron-withdrawing groups in the *para* or *ortho* positions of the phenyl ring were oxidized to the corresponding imines with excellent, 99 or >99 % (**2b**, **2c**, **2d** in Table 5), or good yields, 95 % (**2e**) and 73 % (**2f**) (entries 2–6, Table 5) and the respective functional groups (methoxy, methyl, fluor or acetal) were well tolerated under the afore-mentioned reaction conditions. Heterocyclic methylamines, such as **1g** and **1h** (entries 7–8, Table 5), were also efficiently transformed into the expected self-coupled imines (90–89 %), even though **1h** is known to poison metal catalysts.^[28] Moreover, the oxidation of non-active^[30] secondary benzylamines such as dibenzylamine (**1i**) and 1,2,3,4-tetrahydroisoquinoline (**1j**) proceeded satisfactorily to give the corresponding imines **2a** and **2j** with high yields, >99 and 93 %, respectively (entries 9–10, Table 5). Indeed, the oxidation of the unsymmetrical secondary amine (**1j**) took place in a regioselective manner to give the conjugated N-benzylidene product **2j** (entry 10, Table 5). In additional experiments, full conversion to the desired products was obtained for substrates **1e**, **1f**, **1g** and **1h**, when the photocatalyst loading was increased to 1 mol % (see entries 5–8 in Table 5). By contrast, the application of this protocol to other challenging substrates such as α-methylbenzylamine (**1k**), *n*-hexylamine (**1l**) or 1,2,3,4-tetrahydroquinoline (**1m**) failed to produce the expected imines in agreement with the results reported for other catalytic systems (entries 11,^{[32],[60]} 12^{[61],[62],[63],[64]} and 13^{[26],[65]} in Table 5). Consequently, the presence of either steric hindrance on the α-C as in **1k**, or nonactivated (non-benzylic) α-H, as in **1l** and **1m**, is strongly detrimental for this oxidation. In other words, the lower reactivity of **1l** and **1m** can be rationalized due to the lower acidity of the α-H in these substrates. The regioselectivity in the oxidation of substrate **1j** further supports this interpretation. Nevertheless, the new photocatalysts afford a wide range of secondary aldimines from benzylamines with different functional groups in the aromatic ring in an efficient and smooth manner.

Proposal of a reaction mechanism

We have formulated a detailed mechanistic proposal for the Ru-promoted photooxidative coupling of benzylamines based on both our experimental results (Table 5) and the literature background^[66] (see Scheme 3). This proposal consists of three different processes: (a) photosensitization of ³O₂ to ¹O₂; (b) oxidation of benzylamine to the respective primary aldimine and (c) coupling between the primary aldimine and a second molecule of benzylamine.

FULL PAPER

Table 5. Photooxidation experiments on amines **1a-1m** with **[RuL3]Cl** or **[RuL5]Cl** under an O₂ atmosphere and blue-LED irradiation ($\lambda = 460$ nm).^[a]

Entry	Substrate	PC	Product	Time (h)	Yield (%)
1		[RuL3]Cl		14	> 99
2		[RuL3]Cl		14	> 99
3		[RuL3]Cl		14	> 99
4		[RuL5]Cl		14	99
5		[RuL3]Cl		14	95 (>99) ^[b]
6		[RuL3]Cl		14	73 (> 99) ^[b]
7		[RuL3]Cl		14	90 (> 99) ^[b]
8		[RuL5]Cl		14	89 (>99) ^[b]
9		[RuL3]Cl		14	> 99
10		[RuL5]Cl		14	93
11		[RuL3]Cl		14	0
12		[RuL3]Cl		14	0
13		[RuL3]Cl		14	0

[a] Reaction conditions: Amines **1a-1m** (10 mM), **[RuL3]Cl** or **[RuL5]Cl** (10⁻² mM, 0.1 mol %), CH₃CN (0.5 mL) at room temperature, under a saturated atmosphere of O₂ and under irradiation with blue light (LED, $\lambda = 460$ nm, 24 W) during 14 h in a septum-capped tube. Conversion yields were determined by ¹H NMR analysis of the crude mixture as average values of two independent experiments. Overoxidation and/or hydrolysis products were not detected in any case.

[b] **[RuL3]Cl** or **[RuL5]Cl** (1 mol %).

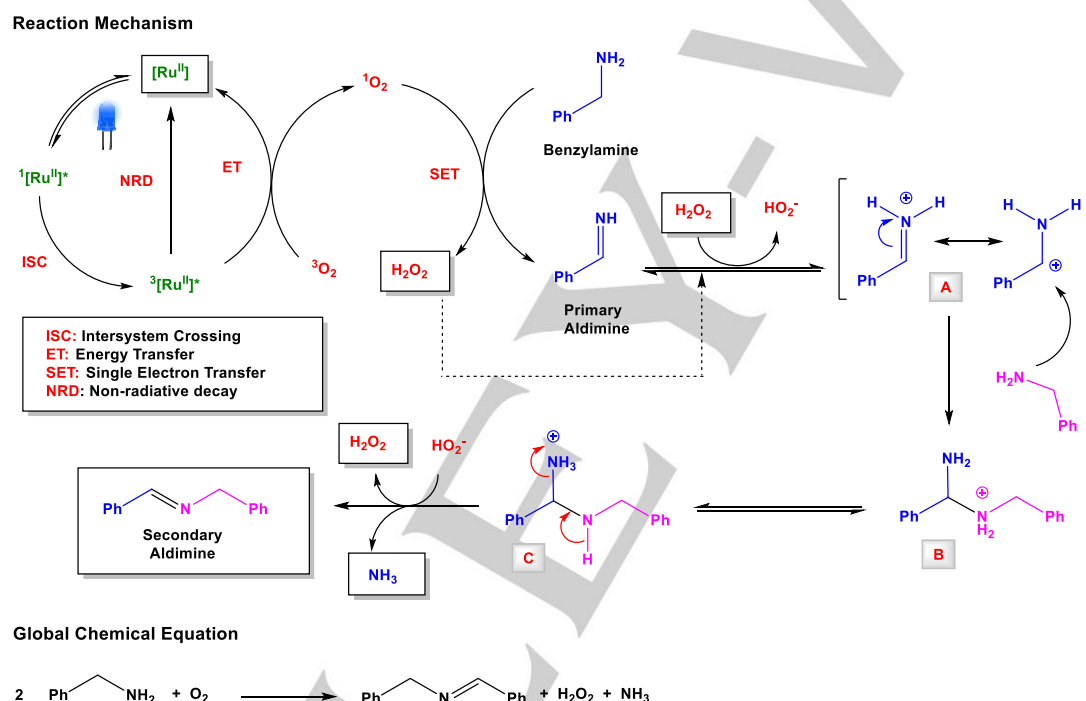
FULL PAPER

(a) Photosensitization. We postulate that the prototypical Ru(II) photocatalyst, [Ru^{II}], absorbs photons under irradiation with blue light to reach an excited singlet state, ¹[Ru^{II}]*, which then undergoes intersystem crossing to the lowest-energy triplet excited state, T₁ = ³[Ru^{II}]*. Afterwards, ³O₂ quenches ³[Ru^{II}]* through an energy transfer process to generate ¹O₂ (Scheme 3) as revealed by experimental evidences (see Table 7).

(b) Oxidation. As detailed in Scheme 4, we propose that the oxidation of benzylamine by ¹O₂, first, involves the formation of a charge-transfer exciplex^[66] between singlet oxygen and the amine based on the electrophilic nature of singlet oxygen^[67–69] and the nucleophilic character of the amine substrate. This step is followed by two sequential single electron transfer (SET) steps and two internal proton transfer (PT) processes and gives rise to the primary aldimine and one molecule of H₂O₂. The acidity of the α-H in intermediate III when using benzylamines (vs. alkyl- or arylamines) is crucial as proved by the negative results obtained with

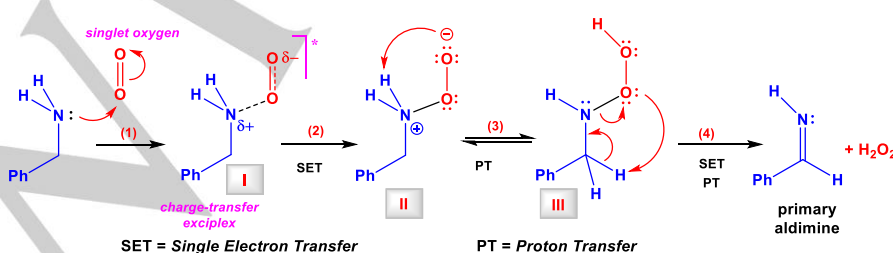
substrates **1l** and **1m** and by the regioselective oxidation of **1j**. Seeberger *et al.* postulated the formation of superoxide as an intermediate in the mechanism for the photosensitized oxidation of dibenzylamines mediated by ¹O₂ in the presence of Ir(III) PCs.^[66] However, our experimental results rule out the formation of this species under the conditions of our protocol.

(c) Amine-imine coupling. Next, we propose the activation of the primary aldimine by in situ formed acidic H₂O₂,^[70] which generates intermediate **A**. Consequently, the electrophilic carbon atom of the protonated aldimine **A** undergoes an attack by the nucleophilic N atom of a second molecule of benzylamine to give the amine-ammonium intermediate **B**. After that, we suggest an internal proton transfer process that forms species **C** where -NH₃⁺ is a very good leaving group. Consequently, the release of NH₃ is strongly favoured affording the final product (secondary aldimine) and regenerating the acidic catalyst H₂O₂ (see Scheme 3).



Scheme 3. Mechanism for the photocatalytic oxidative self-coupling of benzylamine to give the corresponding N-benzylimine in the presence of the Ru(II) photosensitizers and mediated by ¹O₂ and global chemical equation for the same process.

Oxidation Step (Electron Transfer Step)



Scheme 4. Mechanism for the electron transfer step, i.e. oxidation step of benzylamine to the primary aldimine.

FULL PAPER

In consequence, three key features must be highlighted in this mechanism: the photosensitizing ability of the Ru(II) complexes that promotes the production of $^1\text{O}_2$; the electrophilic nature of $^1\text{O}_2$ that facilitates its reaction with nucleophilic amines and the weak acidic character of the *in situ* generated H_2O_2 that assists in the catalytic activation of the primary aldimine.

Transient Absorption Spectroscopy Measurements.

In order to investigate the quenching process in which the triplet excited states of complexes **[RuL3]Cl** and **[RuL5]Cl** are involved, their transient absorption spectra were acquired in the absence and in the presence of O_2 and are presented in Figure SI26 (in orange). The spectral range above 365 nm reveals a negative optical density variation (ΔOD). This bleach means that the ground state extinction coefficient is higher than the excited state extinction coefficient along that range. On the other hand, at 320 nm, the transient spectra exhibit a positive ΔOD , because there is an absorption band of the excited state with a stronger absorption coefficient than the ground state absorption band (Figure SI26). UV-Vis absorption spectra for **[RuL3]Cl** and **[RuL5]Cl** remained unchanged before and after Transient Absorption Spectroscopy experiments, indicating that no photodegradation occurred throughout the full set of experiments (Figure SI27).

Figure 6 features the kinetic traces corresponding to the excited states of **[RuL3]Cl** and **[RuL5]Cl** at 320 nm (absorption decay) and 435 nm (bleach recovery) in deaerated acetonitrile solutions. Both traces go back to zero with the same rate constant for each complex (see Table 6). Moreover, the respective kinetic traces in the presence of oxygen return fully to baseline, as well (Figure SI28). The total recovery of the observed transients to the ground state in the very short time scale of the measurements makes us confident to assign the quenching by oxygen to energy transfer. The ground state recovery furthermore is fitted with a single exponential law. The absence of any observable intermediate species and the total recovery of traces (final ΔOD is zero) suggests that photoinduced electron transfer to produce superoxide either does not exist or does not lead to the escape of superoxide due to fast recombination to the same initial ground state reactants.

Recorded decay rates at 320 nm for both compounds, on aerated and degassed conditions, are presented in Table 6. Although the lifetimes are very short (close to the laser pulse width) which introduces an error in the absolute lifetime values obtained without deconvolution of the laser pulse, there is a reproducible difference between the lifetimes of the transient at 320 nm in the presence and absence of oxygen, compatible with quenching by oxygen. Using a simple Stern-Volmer analysis (eq. 1):

$$\tau_0/\tau = 1 + k_q \cdot \tau_0 \cdot [\text{O}_2] \quad (\text{eq. 1})$$

where τ_0 is the lifetime in degassed solutions; τ , is the lifetime in aerated condition and $[\text{O}_2]$ is the concentration of O_2 found in air equilibrated acetonitrile solutions ($[\text{O}_2] = 2.34 \times 10^{-3}$ M at room temperature),^[71] it is possible to calculate the rate constant for the quenching by oxygen process, k_q (Table 6). The quenching rate constants obtained in this way are of the same order of magnitude as the value known for oxygen diffusion in acetonitrile (1.9×10^{10} L·mol⁻¹·s⁻¹) at room temperature.^[71]

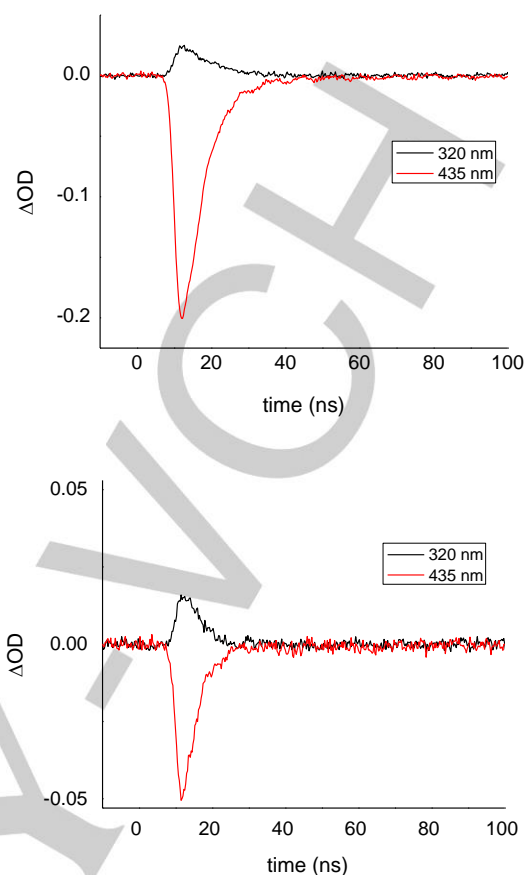


Figure 6. Time-resolved transients at 320 nm (absorption decay) and 435 nm (bleach recovery) recorded ($\lambda_{\text{ex}} = 355$ nm) for deaerated acetonitrile solutions of **[RuL3]Cl** (up) and **[RuL5]Cl** (Bottom).

Table 6. Summary of recorded decay-times of the transients observed at 320 nm in acetonitrile ($A(\lambda_{\text{ex}} = 355 \text{ nm}) \sim 0.2$) for **[RuL3]Cl** and **[RuL5]Cl** and calculated quenching rate constants.

Compound	Lifetimes at 320 nm (ns)		k_q (L·mol ⁻¹ ·s ⁻¹)
	without O_2	with O_2	
[RuL3]Cl	7.9	6.0	1.7×10^{10}
[RuL5]Cl	4.6	3.9	1.6×10^{10}

Detection of H_2O_2 . H_2O_2 was detected by ^1H NMR (CD_3CN) as a broad peak between 8.3 and 8.7 ppm in the reaction crude mixtures obtained for the photocatalytic oxidation of substrates **1a-1j** (except **1g**) in close to an equimolar ratio with respect to each imine product (Figures SI16-SI24).^[17] This experimental evidence further supports the mechanism detailed in Scheme 3 and Scheme 4. Alternative pathways have been described in the literature for the photocatalytic oxidation of benzylamines in the presence of O_2 , but either they do not involve the formation of hydrogen peroxide^[29] or propose that the *in situ* generated H_2O_2 acts as a secondary oxidant and therefore is consumed.^[27]

FULL PAPER

Table 7. Experimental evidences for the participation of $^1\text{O}_2$ in the photooxidation of benzylamines promoted by the new Ru(II) **PCs**.

Entry	Evidences	Experiment
1	Low conversion in the presence of DABCO.	Table 3 (entry 6)
2	Higher conversion in the presence of deuterated acetonitrile.	Table 4 (compare entries 14 and 16)
3	Total decay of [RuL3]Cl transients in the presence of O_2 .	TAS experiments

Conclusion

In summary, we have designed and prepared five new Ru(II) polypyridyl complexes and three related Ir(III) biscyclometalated derivatives bearing N-(arylsulfonyl)-8-amidoquinolate ligands, as potential photocatalysts. The Ru(II) **PSs** exhibit moderate or excellent photostability under blue light irradiation, whereas their Ir(III) counterparts are very light-sensitive. The Ru(II) complexes harvest visible light efficiently but are non-emissive, which could be related to the low $S_0 \leftarrow T_1$ energy gap as shown by DFT calculations and electrochemical data. Furthermore, we have demonstrated that the Ru(II) **PCs** display excellent photocatalytic activity in the O_2 -mediated oxidation of primary or secondary benzylamines, despite being non-emissive. The Ir(III) derivatives are less efficient photosensitizers likely due to their photosensitivity. More specifically, the protocol for the preparation of the corresponding secondary aldimines is green, safe, efficient and highly selective, given that it requires low catalyst loadings, low O_2 pressure and works smoothly at room temperature, providing excellent yields of the imine products in short times. In addition, it can be applied to a wide variety of substrates with different functional groups, while no over-oxidation or hydrolysis side-products are formed in any case. Finally, for this transformation, we propose a detailed mechanism mediated by $^1\text{O}_2$ as the actual oxidant in view of the experimental results (TAS measurements and others). As a logical corollary of this work we have demonstrated that the use of monoanionic N-(arylsulfonyl)-8-amidoquinolate ligands in the design of polypyridyl Ru(II) complexes shortens their $S_0 \leftarrow T_1$ energy gap relative to $[\text{Ru}(\text{bpy})_3]^{2+}$, which in turn, improves their visible light harvesting ability at the expense of a non-emissive behaviour. Nonetheless, the resulting complexes are still active photocatalysts, likely owing to the fact that the photosensitizing process is faster than the non-radiative decay. Conclusively, we believe that this work could pave the way for the study of the photocatalytic activity of similar monocationic $[\text{Ru}(\text{bpy})_2(\text{N}^-\text{A})]^+$ complexes or even other non-emissive dyes.

Experimental Section

General experimental procedure for the synthesis of ligands HL1-HL6

In a 100 mL Schlenk flask, 8-aminoquinoline (1.615 mmol) was dissolved in dichloromethane (12 mL). Then, triethylamine (2.418 mmol) was added to the solution at 0°C and the mixture was stirred for 10 minutes. After that, in a different 100 mL Schlenk flask, the appropriate arylsulfonyl chloride

(2.423 mmol) was dissolved in dichloromethane (12 mL), cooled with an ice bath and stirred for a few minutes. Then, this solution was added slowly at 0°C over the first one, and the resulting solution was stirred at room temperature for 22 h under nitrogen atmosphere. The evolution of the reaction was monitored by TLC. Subsequently, an aqueous saturated solution of NaHCO_3 (3 x 20 mL) was added to extract the inorganic salts. The organic phase was separated and dried over MgSO_4 . After that, the suspension was filtered, and the filtrate was concentrated under reduced pressure. Finally, the crude mixture was purified by column chromatography on silica gel ($\text{CH}_2\text{Cl}_2/\text{AcOEt}$, (10:1)) to obtain the desired pure ligands.

General experimental procedure for the synthesis of complexes **[RuL1]Cl**-**[RuL5]Cl**

In a 100 mL Schlenk flask, previously purged with nitrogen, the corresponding pro-ligand (0.170 mmol) and *rac-cis*- $[\text{Ru}(\text{bpy})_2\text{Cl}_2]\cdot 2\text{H}_2\text{O}$ (0.170 mmol) were dissolved in ethanol (19 mL). Then, NaHCO_3 (0.849 mmol) was added and the suspension was stirred under reflux at 90°C for 20 h under nitrogen atmosphere. The resulting mixture was cooled at room temperature and filtered to remove the excess of NaHCO_3 . After that, its volume was reduced by evaporating the solvent under reduced pressure. The product was precipitated with diethyl ether (10 mL) and filtered. The dark red solid crude was washed with water (5 mL), diethyl ether (5 mL), filtered and dried under vacuum.

General experimental procedure for the synthesis of complexes **[IrL1]**, **[IrL4]** and **[IrL5]**

In a 100 mL Schlenk flask, previously purged with nitrogen, the corresponding pro-ligand (0.186 mmol) and *rac*- $[\text{Ir}(\mu\text{-Cl})(\text{ppy})_2]_2$ (0.094 mmol) were dissolved in 18 mL of a mixture of $\text{CH}_2\text{Cl}_2/\text{MeOH}$ (8:10). An excess of NaHCO_3 (0.932 mmol, 1:5 with respect to the respective pro-ligand) was added, and the suspension was stirred and refluxed at 60°C for 24 h under nitrogen atmosphere. The resulting mixture was cooled at room temperature and the solvents were evaporated under reduced pressure. Then, the crude solid was washed with water (2 x 3 mL) and *n*-hexane (2 x 3 mL) and dried under vacuum for 4 h.

X-ray crystallography

Data collection and refinement parameters for **[RuL4]PF₆** are summarized in Table S13 of the Supporting Information. A single crystal of the complex was coated with high-vacuum grease, mounted on a glass fiber, and transferred to a Bruker SMART APEX CCD-based diffractometer equipped with a graphite-monochromated MoK α radiation source ($\lambda = 0.71073$ Å). The highly redundant datasets were integrated with SAINT^[72] and corrected for Lorentzian and polarization effects. The absorption correction was based on the function fitting to the empirical transmission surface as sampled by multiple equivalent measurements with the program SADABS.^[73] The software package WingX^[74] was used for space-group determination, structure solution, and OLEX 2 1.2.10^[75] was used for refinement by full-matrix least-squares methods based on F². A successful solution by direct methods provided most non-hydrogen atoms from the E map. The remaining non-hydrogen atoms were located in an alternating series of least squares cycles and difference Fourier maps. All non-hydrogen atoms were refined with anisotropic displacement coefficients. Hydrogen atoms were placed by using a riding model and included in the refinement at calculated positions.

CCDC 1970014 **[RuL4]PF₆** contains the supplementary crystallographic data for this paper. These data are provided free of charge by The Cambridge Crystallographic Data Centre.

FULL PAPER

Theoretical calculations

Density functional theory (DFT) calculations were carried out with the D.01 revision of the Gaussian 09 package,^[76] using the Becke's three-parameter B3LYP exchange-correlation functional,^[77,78] together with the 6-31G(d,p) basis set for H, C, N, O, F, and S,^[79,80] and the "double- ξ " quality LANL2DZ basis set for the Ru element.^[81] The geometries of the singlet ground state (S_0) and the lowest-energy triplet state (T_1) were fully optimized without imposing any symmetry restriction. The geometries of the triplet states were calculated at the spin-unrestricted UB3LYP level with a spin multiplicity of 3. All the calculations were performed in the presence of the solvent (acetonitrile). Solvent effects were considered within the self-consistent reaction field (SCRF) theory using the SMD keyword that performs a polarized continuum model (PCM)^[82] calculation using the solvation model of Thrun et al.^[83] Time-dependent DFT (TD-DFT) calculations of the lowest-lying 15 singlets and triplets were performed in the presence of the solvent at the minimum-energy geometry optimized for the ground state (S_0).

Electrochemical measurements

Electrochemical measurements were performed using a portable Bipotentiostat μ STAT 300 (DropSens) equipment controlled by DropView (DropSens). All experiments were carried out using a three-electrode cell, namely: a glassy-carbon disk with a diameter of 3 mm as the working electrode, a platinum wire as the auxiliary electrode, and a RE-5B Ag/AgCl (BASi) reference electrode. Oxygen was removed from the solution by bubbling argon for 10 min and keeping the argon atmosphere along the whole experiment. The measurements were recorded for acetonitrile solutions of the complexes (10^{-3} M) in the presence of [n Bu₄N][PF₆] (0.1 M) as the supporting electrolyte by cyclic voltammetry (CV) at a scan rate of 100 mV s⁻¹ in a clockwise direction. Ferrocene was added at the end of all the experiments as the internal reference in order to refer the potentials to the redox pair ferrocenium/ferrocene (Fc^+/Fc) under the conditions of our experiments. The potential experimentally determined for the redox couple Fc^+/Fc was $E^{\circ}_{1/2} = 0.46 \pm 0.005$ V vs. Ag/AgCl. Therefore, the experimental redox potentials were calculated from the corresponding voltammograms as: E° (vs AgCl/Ag) = ($E_{ap} + E_{cp}$)/2, for reversible peaks where E_{ap} and E_{cp} stand for anodic and cathodic peak potentials, respectively. However, for irreversible peaks, the potentials were calculated as either the E_{ap} maximum or E_{cp} minimum. E° (vs Fc^+/Fc) = E° (vs AgCl/Ag) - 0.443, for potential values reported in reference to the (Fc^+/Fc) redox couple.

General procedure for photocatalytic oxidation

In a septum-capped tube the amine (5 μ mol in solution of CH₃CN), the PC (Photocatalyst = 0.005 or 0.05 μ mol in solution of CH₃CN), and additional CH₃CN to providing the desired final concentration of substrate (10 mM in 0.5 mL), were placed. The system was purged with O₂ or N₂ until atmosphere saturation and irradiated with Blue LED light ($\lambda = 460$ nm, 24W) at room temperature during the required time. Then, an aliquot (100 μ L) of the reaction mixture was diluted in CD₃CN (400 μ L) and the mixture was analysed by ¹H NMR to determine the conversion. The yield values for the imines were calculated from the integration of the peaks assigned to the methylene groups of both the imine product (e.g.: doublet at 4.75 ppm for Ph-CH₂-N=CH-Ph, **2a**) and the benzyl amine used as reactant (e.g.: singlet at 3.78 ppm for Ph-CH₂-NH₂, **1a**).

TAS Measurements

Solutions of [RuL3]Cl and [RuL5]Cl in acetonitrile were prepared, and the corresponding absorption spectra in 1 cm quartz cuvettes were acquired. Absorbance at $\lambda_{ex} = 355$ nm (laser flash photolysis excitation source) were subsequently adjusted to match a value of approximately 0.2. Degassing of samples was achieved by performing three freeze-pump-thaw cycles on each of the samples, prior to laser flash photolysis. Transient absorption spectra of [RuL3]Cl and [RuL5]Cl were measured using a flash photolysis

setup composed of a LKS 60 ns laser photolysis spectrometer from Applied Photophysics, with a Brilliant Q-Switch Nd:YAG laser from Quantel, using the third harmonics ($\lambda_{ex} = 355$ nm, laser pulse half-width equal to 4 ns). Measurements were repeated in degassed and aerated samples.

Acknowledgements

We gratefully acknowledge the financial support provided by the Spanish Ministerio de Ciencia, Innovación y Universidades (RTI2018-100709-B-C21 and CTQ (QMC)- RED2018-102471-T) and Junta de Castilla y León (BU087G19). M. V. is grateful for the financial support received from the Consejería de Educación-Junta de Castilla y León-FEDER (BU042U16-BU305P18).

We are also indebted to Pilar Castroviejo and Marta Mansilla (PCI of the Universidad de Burgos) and Javier Pérez (Photophysics Unit of Institute of Chemical Research of Catalonia (ICIQ)) for the technical support and Dr. José Vicente Cuevas Vicario for his advices regarding theoretical calculations.

Keywords: Ru(II) polypyridyl complexes • Sulfonamides • Photooxidation of amines • Photocatalysis • Singlet oxygen.

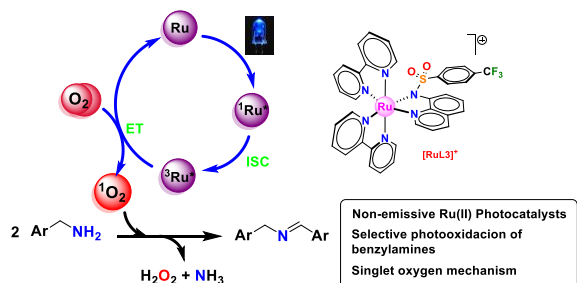
- [1] D. M. Schultz, T. P. Yoon, *Science* **2014**, 343, 1239176.
- [2] M. H. Shaw, J. Twilton, D. W. C. MacMillan, *J. Org. Chem.* **2016**, 81, 6898–6926.
- [3] C. B. Kelly, N. R. Patel, D. N. Primer, M. Jouffroy, J. C. Tellis, G. A. Molander, *Nat. Protoc.* **2017**, 12, 472–492.
- [4] C. K. Prier, D. A. Rankin, D. W. C. MacMillan, *Chem. Rev.* **2013**, 113, 5322–5363.
- [5] S.-I. Murahashi, *Angew. Chem., Int. Ed* **1995**, 34, 2443–2465.
- [6] S. Kobayashi, H. Ishitani, *Chem. Rev.* **1999**, 99, 1069–1094.
- [7] K. Yamada, K. Tomioka, *Chem. Rev.* **2008**, 108, 2874–2886.
- [8] T. Sonobe, K. Oisaki, M. Kanai, *Chem. Sci.* **2012**, 3, 3249–3255.
- [9] V. V. Kouznetsov, C. E. P. Galvis, *Tetrahedron* **2018**, 74, 773–810.
- [10] R. W. Layer, *Chem. Rev.* **1963**, 63, 489–510.
- [11] K. C. Nicolaou, C. J. N. Mathison, T. Montagnon, *Angew. Chemie* **2003**, 115, 4211–4216.
- [12] K. Marui, A. Nomoto, H. Akashi, A. Ogawa, *Synthesis* **2015**, 48, 31–42.
- [13] B. Zhu, R. J. Angelici, *Chem. Commun.* **2007**, 2157–2159.
- [14] M. Rueping, C. Vila, A. Szadkowska, R. M. Koenigs, J. Fronert, *ACS Catal.* **2012**, 2, 2810–2815.
- [15] G. Jiang, J. Chen, J. S. Huang, C. M. Che, *Org. Lett.* **2009**, 11, 4568–4571.
- [16] H. Yu, J. Wang, Y. Zhai, M. Zhang, S. Ru, S. Han, Y. Wei, *ChemCatChem* **2018**, 10, 4274–4279.
- [17] J. H. Park, K. C. Ko, E. Kim, N. Park, J. H. Ko, D. H. Ryu, T. K. Ahn, J. Y. Lee, S. U. Son, *Org. Lett.* **2012**, 14, 5502–5505.
- [18] H. Ho, K. Manna, A. D. Sadow, *Angew. Chem., Int. Ed.* **2012**, 51, 8607–8610.
- [19] J. Jin, H.-W. Shin, J. H. Park, J. H. Park, E. Kim, T. K. Ahn, D. H. Ryu, S. U. Son, *Organometallics* **2013**, 32, 3954–3959.
- [20] Y. H. Li, X. Le Liu, Z. T. Yu, Z. S. Li, S. C. Yan, G. H. Chen, Z. G. Zou, *Dalton Trans.* **2016**, 45, 12400–12408.
- [21] T. N. Zehnder, O. Blacque, K. Venkatesan, *Dalton. Trans.* **2014**, 43, 11959–11972.
- [22] A. Berlicka, B. König, *Photochem. Photobiol. Sci.* **2010**, 9, 1359–1366.
- [23] L. Huang, J. Zhao, S. Guo, C. Zhang, J. Ma, *J. Org. Chem.* **2013**, 78,

FULL PAPER

- 5627–5637.
- [24] J. Ye, K. Ni, J. Liu, G. Chen, M. Ikram, Y. Zhu, *ChemCatChem* **2018**, *10*, 259–265.
- [25] Z. Wang, X. Lang, *Appl. Catal. B Environ.* **2018**, *224*, 404–409.
- [26] S. Furukawa, Y. Ohno, T. Shishido, K. Teramura, T. Tanaka, *ACS Catal.* **2011**, *1*, 1150–1153.
- [27] F. Su, S. C. Mathew, L. Möhlmann, M. Antonietti, X. Wang, S. Blechert, *Angew. Chem., Int. Ed.* **2011**, *50*, 657–660.
- [28] F. Raza, J. H. Park, H. R. Lee, H. I. Kim, S. J. Jeon, J. H. Kim, *ACS Catal.* **2016**, *6*, 2754–2759.
- [29] L. Ye, Z. Li, *ChemCatChem* **2014**, *6*, 2540–2543.
- [30] C. Su, R. Tandiana, B. Tian, A. Sengupta, W. Tang, J. Su, K. P. Loh, *ACS Catal.* **2016**, *6*, 3594–3599.
- [31] Y. Zhi, K. Li, H. Xia, M. Xue, Y. Mu, X. Liu, *J. Mater. Chem. A* **2017**, *5*, 8697–8704.
- [32] X. Yang, T. Huang, S. Gao, R. Cao, *J. Catal.* **2019**, *378*, 248–255.
- [33] K. Teegardin, J. I. Day, J. Chan, J. Weaver, *Org. Process Res. Dev.* **2016**, *20*, 1156–1163.
- [34] K. T. Ngo, N. A. Lee, S. D. Pinnace, D. J. Szalda, R. T. Weber, J. Rochford, *Inorg. Chem.* **2016**, *55*, 2460–2472.
- [35] N. Thrimurtulu, R. Nallagonda, C. M. R. Volla, *Chem. Commun.* **2017**, *53*, 1872–1875.
- [36] Y. Ran, Y. Yang, L. Zhang, *Tetrahedron Lett.* **2016**, *57*, 3322–3325.
- [37] L. E. da Silva, A. C. Joussef, L. K. Pacheco, D. G. da Silva, M. Steindel, R. A. Rebelo, *Bioorg. Med. Chem.* **2007**, *15*, 7553–7560.
- [38] S. Dayan, N. Ozpozan Kalaycioglu, J.-C. Daran, A. Labande, R. Poli, *Eur. J. Inorg. Chem.* **2013**, *2013*, 3224–3232.
- [39] S. Dayan, N. Kalaycioglu Özpozan, *Inorganica Chim. Acta* **2018**, *474*, 81–88.
- [40] A. Y. Shabalin, N. Y. Adonin, V. V. Bardin, S. A. Prikhod'ko, M. N. Timofeeva, M. V. Bykova, V. N. Parmon, *J. Fluor. Chem.* **2013**, *149*, 82–87.
- [41] S. Kumar, Y. Hisamatsu, Y. Tamaki, O. Ishitani, S. Aoki, *Inorg. Chem.* **2016**, *55*, 3829–3843.
- [42] C. Alter, B. Neumann, H.-G. Stammer, B. Hoge, *Eur. J. Inorg. Chem.* **2018**, *2018*, 867–875.
- [43] S. Miyaniishi, T. Yamaguchi, *New J. Chem.* **2017**, *41*, 8036–8044.
- [44] D. R. Whang, K. Sakai, S. Y. Park, *Angew. Chem., Int. Ed.* **2013**, *52*, 11612–11615.
- [45] K. Suzuki, A. Kobayashi, S. Kaneko, K. Takehira, T. Yoshihara, H. Ishida, Y. Shiina, S. Oishi, S. Tobita, *Phys. Chem. Chem. Phys.* **2009**, *11*, 9850–9860.
- [46] H. Iranmanesh, K. S. A. Arachchige, M. Bhadbhade, W. A. Donald, J. Y. Liew, K. T. C. Liu, E. T. Luis, E. G. Moore, J. R. Price, H. Yan, et al., *Inorg. Chem.* **2016**, *55*, 12737–12751.
- [47] S. Bellinger-Buckley, T.-C. Chang, S. Bag, D. Schweinfurth, W. Zhou, B. Torok, B. Sarkar, M.-K. Tsai, J. Rochford, *Inorg. Chem.* **2014**, *53*, 5556–5567.
- [48] D. P. Rillema, G. Allen, T. J. Meyer, D. Conrad, *Inorg. Chem.* **1983**, *22*, 1617–1622.
- [49] J. Torres, M. C. Carrión, J. Leal, F. A. Jalón, J. V. Cuevas, A. M. Rodríguez, G. Castañeda, B. R. Manzano, *Inorg. Chem.* **2018**, *57*, 970–984.
- [50] T. C. Motley, L. Troian-Gautier, M. K. Brennaman, G. J. Meyer, *Inorg. Chem.* **2017**, *56*, 13579–13592.
- [51] P. K. Chow, C. Ma, W. To, G. S. M. Tong, S. Lai, S. C. F. Kui, W. Kwok, C. Che, *Angew. Chem., Int. Ed.* **2013**, *52*, 11775–11779.
- [52] V. V. Patil, E. M. Gayakwad, G. S. Shankarling, *J. Org. Chem.* **2016**, *81*, 781–786.
- [53] M. Singh, A. K. Yadav, L. D. S. Yadav, R. K. P. Singh, *Tetrahedron Lett.* **2018**, *59*, 450–453.
- [54] M. Vaquero, A. Ruiz-Riaguas, M. Martínez-Alonso, F. A. Jalón, B. R. Manzano, A. M. Rodríguez, G. García-Herbosa, A. Carbayo, B. García, G. Espino, *Chem. – A Eur. J.* **2018**, *24*, 10662–10671.
- [55] G. R. Seely, *J. Phys. Chem.* **1969**, *73*, 125–129.
- [56] K. Tateno, R. Ogawa, R. Sakamoto, M. Tsuchiya, T. Otani, T. Saito, *Org. Lett.* **2014**, *16*, 3212–3215.
- [57] T. Ueno, Y. Urano, H. Kojima, T. Nagano, *J. Am. Chem. Soc.* **2006**, *128*, 10640–10641.
- [58] T. Nevesely, E. Svobodová, J. Chudoba, M. Sikorski, R. Cibulka, *Adv. Synth. Catal.* **2016**, *358*, 1654–1663.
- [59] P. R. Ogilby, C. S. Foote, *J. Am. Chem. Soc.* **1983**, *105*, 3423–3430.
- [60] L. M. Aguirre-Díaz, N. Snejko, M. Iglesias, F. Sánchez, E. Gutiérrez-Puebla, M. Á. Monge, *Inorg. Chem.* **2018**, *57*, 6883–6892.
- [61] B. Chen, L. Wang, W. Dai, S. Shang, Y. Lv, S. Gao, *ACS Catal.* **2015**, *5*, 2788–2794.
- [62] A. Kumar, A. M. Sadanandhan, S. L. Jain, *New J. Chem.* **2019**, *43*, 9116–9122.
- [63] R. Brisar, D. Hollmann, E. Mejia, *European J. Org. Chem.* **2017**, *2017*, 5391–5398.
- [64] Y. R. Girish, R. Biswas, M. De, *Chem. - A Eur. J.* **2018**, *24*, 13871–13878.
- [65] J. Jin, C. Yang, B. Zhang, K. Deng, *J. Catal.* **2018**, *361*, 33–39.
- [66] D. B. Ushakov, M. B. Plutschack, K. Gilmore, P. H. Seeberger, *Chem. - A Eur. J.* **2015**, *21*, 6528–6534.
- [67] F. Jensen, A. Greer, E. L. Clennan, *J. Am. Chem. Soc.* **1998**, *120*, 4439–4449.
- [68] C. S. Foote, J. W. Peters, *J. Am. Chem. Soc.* **1971**, *93*, 3795–3796.
- [69] K. L. Stensaas, B. V. McCarty, N. M. Touchette, J. B. Brock, *Tetrahedron* **2006**, *62*, 10683–10687.
- [70] $\neq \text{H}_2\text{O}_2$ is a very weak acid but it is more acidic than water $\text{H}_2\text{O}_2 + \text{H}_2\text{O} \rightarrow \text{H}_3\text{O}_2^+ + \text{OH}^-$; $K_a = 2.4 \cdot 10^{-12}$ 20 °C.
- [71] Steven L. Murov, *Handbook of Photochemistry (Handbuch der Photochemie)*. XI, 272 S., 28 Abb., 44 Tab. Marcel Dekker, Inc., New York 1973.
- [72] SAINT+ v7.12a. Area-Detector Integr. Program. Bruker-Nonius AXS. Madison, Wisconsin, USA, 2004. **2004**.
- [73] G. M. Sheldrick, *SADABS A Progr. Empir. Absorpt. Correct. Version 2004/1*; Univ. Göttingen, Göttingen, Ger. **2004**.
- [74] L. J. Farrugia, *J. Appl. Crystallogr.* **2012**, *45*, 849–854.
- [75] O. V. Dolomanov, L. J. Bourhis, R. J. Gildea, J. A. K. Howard, H. Puschmann, *J. Appl. Crystallogr.* **2009**, *42*, 339–341.
- [76] M. J. Frisch, G. W. Trucks, H. B. Schlegel, G. E. Scuseria, M. A. Robb, J. R. Cheeseman, G. Scalmani, V. Barone, B. Mennucci, G. A. Petersson, et al., *Gaussian, Inc. Wallingford CT* **2013**.
- [77] A. D. Becke, *J. Chem. Phys.* **1993**, *98*, 5648–5652.
- [78] C. Lee, W. Yang, R. G. Parr, *Phys. Rev. B* **1988**, *37*, 785–789.
- [79] M. M. Francl, W. J. Pietro, W. J. Hehre, J. S. Binkley, M. S. Gordon, D. J. DeFrees, J. A. Pople, *J. Chem. Phys.* **1982**, *77*, 3654–3665.
- [80] P. C. Hariharan, J. A. Pople, *Theor. Chim. Acta* **1973**, *28*, 213–222.
- [81] P. J. Hay, W. R. Wadt, *J. Chem. Phys.* **1985**, *82*, 299–310.
- [82] G. Scalmani, M. J. Frisch, *J. Chem. Phys.* **2010**, *132*, 114110.
- [83] A. V. Marenich, C. J. Cramer, D. G. Truhlar, *J. Phys. Chem. B* **2009**, *113*, 6378–6396.

FULL PAPER

Entry for the Table of Contents



A family of monocationic non-emissive Ru(II) polypyridyl complexes exhibit efficient and selective photocatalytic activity in the photooxidation of benzylamines to imines. The presence of the formally anionic N-(arylsulfonyl)-8-amidoquinolate ligands enable these dyes to harvest visible light effectively, while their non-emissive behavior is related to their low energy gaps. Experimental evidences suggest that ¹O₂ is the actual oxidant.

Institute and/or researcher Twitter usernames: @MVaqueroG; @UBUinvestiga; @UBUEstudiantes